QUANTUM PHYSICS

Noise-resilient edge modes on a chain of superconducting qubits

X. Mi¹, M. Sonner², M. Y. Niu¹, K. W. Lee¹, B. Foxen¹, R. Acharya¹, I. Aleiner¹, T. I. Andersen¹, F. Arute¹, K. Arya¹, A. Asfaw¹, J. Atalaya¹, J. C. Bardin^{1,3}, J. Basso¹, A. Bengtsson¹, G. Bortoli¹, A. Bourassa¹, L. Brill¹, M. Broughton¹, B. B. Buckley¹, D. A. Buell¹, B. Burkett¹, N. Bushnell¹, Z. Chen¹, B. Chiaro¹, R. Collins¹, P. Conner¹, W. Courtney¹, A. L. Crook¹, D. M. Debroy¹, S. Demura¹, A. Dunsworth¹, D. Eppens¹, C. Erickson¹, L. Faoro¹, E. Farhi¹, R. Fatemi¹, L. Flores¹, E. Forati¹, A. G. Fowler¹, W. Giang¹, C. Gidney¹, D. Gilboa¹, M. Giustina¹, A. G. Dau¹, J. A. Gross¹, S. Habegger¹, M. P. Harrigan¹, M. Hoffmann¹, S. Hong¹, T. Huang¹, A. Huff¹, W. J. Huggins¹, L. B. Ioffe¹, S. V. Isakov¹, J. Iveland¹, E. Jeffrey¹, Z. Jiang¹, C. Jones¹, D. Kafri¹, K. Kechedzhi¹, T. Khattar¹, S. Kim¹, A. Y. Kitaev^{1,4}, P. V. Klimov¹, A. R. Klots¹, A. N. Korotkov^{1,5}, F. Kostritsa¹, J. M. Kreikebaum¹, D. Landhuis¹, P. Laptev¹, K.-M. Lau¹, J. Lee¹, L. Laws¹, W. Liu¹, A. Locharla¹, O. Martin¹, J. R. McClean¹, M. McEwen^{1,6}, B. Meurer Costa¹, K. C. Miao¹, M. Mohseni¹, S. Montazeri¹, A. Morvan¹, E. Mount¹, W. Mruczkiewicz¹, O. Naaman¹, M. Neeley¹, C. Neill¹, M. Newman¹, T. E. O'Brien¹, A. Opremcak¹, A. Petukhov¹, R. Potter¹, C. Quintana¹, N. C. Rubin¹, N. Saei¹, D. Sank¹, K. Sankaragomathi¹, K. J. Satzinger¹, C. Schuster¹, M. J. Shearn¹, V. Shvarts¹, D. Strain¹, Y. Su¹, M. Szalay¹, G. Vidal¹, B. Villalonga¹, C. Vollgraff-Heidweiller¹, T. White¹, Z. Yao¹, P. Yeh¹, J. Yoo¹, A. Zalcman¹, Y. Zhang¹, N. Zhu¹, H. Neven¹, D. Bacon¹, J. Hilton¹, E. Lucero¹, R. Babbush¹, S. Boixo¹, A. Megrant¹, Y. Chen¹, J. Kelly¹, V. Smelyanskiy¹, D. A. Abanin^{1,2}*, P. Roushan¹*

Inherent symmetry of a quantum system may protect its otherwise fragile states. Leveraging such protection requires testing its robustness against uncontrolled environmental interactions. Using 47 superconducting qubits, we implement the one-dimensional kicked Ising model, which exhibits nonlocal Majorana edge modes (MEMs) with \mathbb{Z}_2 parity symmetry. We find that any multiqubit Pauli operator overlapping with the MEMs exhibits a uniform late-time decay rate comparable to single-qubit relaxation rates, irrespective of its size or composition. This characteristic allows us to accurately reconstruct the exponentially localized spatial profiles of the MEMs. Furthermore, the MEMs are found to be resilient against certain symmetry-breaking noise owing to a prethermalization mechanism. Our work elucidates the complex interplay between noise and symmetry-protected edge modes in a solid-state environment.

he symmetry of a quantum system can give rise to topologically distinct degenerate ground states. A quantum superposition of such states is, in principle, immune to dephasing; additionally, an energy gap separates the ground states from the excited states and further protects the ground states from energy decay. As such, symmetryprotected ground states may form decoherencefree subspaces (1-4) and are promising candidates for topological quantum computing (5, 6). An example model supporting symmetry-protected topological states is the Kitaev model of spinless fermions in a one-dimensional (1D) wire (7). The \mathbb{Z}_2 parity symmetry of the model leads to a pair of degenerate ground states. The distinct parities of the two ground states protect them against local parity-preserving noise, such as potential fluctuations (8). The topological property of these degenerate ground states is commonly

¹Google Research, Mountain View, CA, USA. ²Department of Theoretical Physics, University of Geneva, Geneva, Switzerland. ³Department of Electrical and Computer Engineering, University of Massachusetts, Amherst, MA, USA. ⁴Institute for Quantum Information and Matter, California Institute of Technology, Pasadena, CA, USA. ⁵Department of Electrical and Computer Engineering, University of California, Riverside, CA, USA. ⁶Department of Physics, University of California, Santa Barbara, CA, USA.

*Corresponding author. Email: banin@google.com (D.A.A.); pedramr@google.com (P.R.)

described by a pair of localized Majorana edge modes (MEMs) at the ends of the wire.

Whereas the degree of symmetry protection in a closed quantum system is often understood, experimental quantum systems are invariably subject to physical noise sources that do not necessarily respect the underlying symmetry. In the context of MEMs, notable efforts have been directed toward experimentally realizing the Kitaev model, for example, in nanowires with spin-orbit interactions placed in the proximity of a superconductor (9-16). Here, the underlying \mathbb{Z}_2 symmetry cannot be broken by local perturbations within a closed system. Nevertheless, theoretical results have widely suggested that MEMs remain susceptible to a variety of decoherence effects from their open solid-state environment (17-20). Experimental results have also established that the density of subgap quasiparticles is often orders of magnitude higher than predictions from simple thermal population arguments (21-24). The incoherent processes involving these quasiparticles can change the parity of the ground state and, consequently, destroy the topological protection. These results highlight the importance of characterizing the extent of symmetry protection in realistic open-system environments.

The advent of high-fidelity quantum processors and simulators suggests an alternative

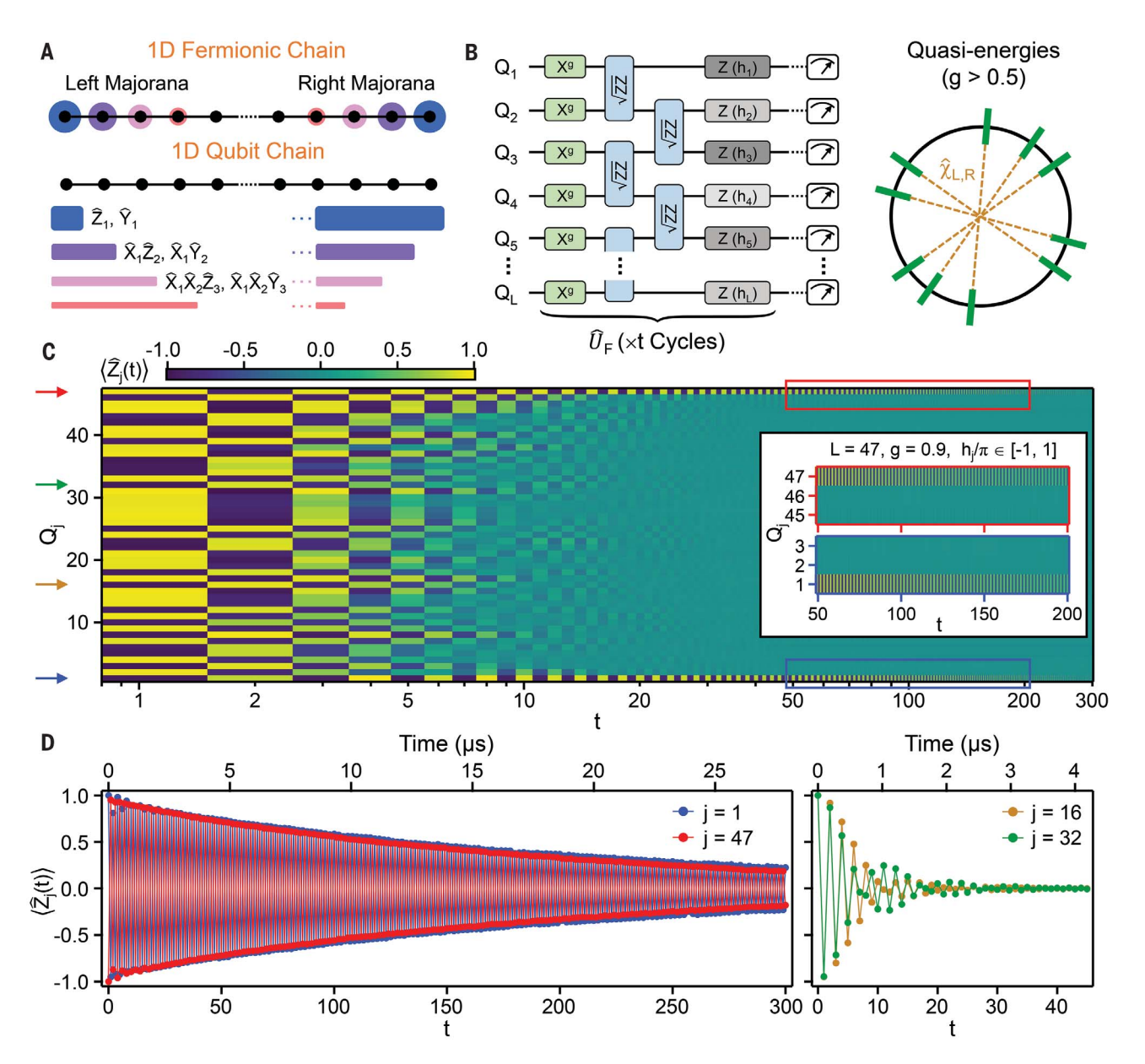
approach to examining the realistic extent of protection for a given symmetry (25-27). In this study, we use the Jordan-Wigner transformation (JWT) to map the Kitaev model to a transverse Ising spin model (28), which is more compatible with a chain of qubits (29-32). The JWT also maps each MEM, commonly represented by a sum of local Majorana operators in the fermionic chain, to a sum of Pauli spin operators that can be individually characterized on a quantum processor. Given the nonlocal nature of the JWT, the MEMs in the Pauli basis are prone to local symmetry-breaking noise even within a closed system, which distinguishes them from MEMs in fermionic systems. Despite this disadvantage, we find that the interplay between \mathbb{Z}_2 parity symmetry and a prethermalization mechanism endows the MEMs with a strong resilience toward both closed-system thermalization and opensystem perturbations such as low-frequency noise. Furthermore, we discover a method for accurately reconstructing the Pauli expansion of MEMs in the presence of decoherence, which may be extended to study other integrals of motion in many-body quantum systems.

The experiment is conducted on an openended chain of L=47 superconducting qubits [see (33) for device details]. The qubit chain is periodically driven by a quantum circuit corresponding to a kicked Ising model (Fig. 1B), with the following unitary applied in each cycle

$$\hat{U}_{\mathrm{F}} = e^{-\frac{i}{2}\sum\limits_{j=1}^{L}h_{j}\hat{Z}_{j}} e^{-\frac{i\pi J}{2}\sum\limits_{j=1}^{L-1}\hat{Z}_{j}Z_{j+1}} e^{-\frac{i\pi g}{2}\sum\limits_{j=1}^{L}\hat{X}_{j}}$$
 (1)

where \hat{X}_i and \hat{Z}_i denote Pauli operators acting on a given qubit Q_i . Here J and g denote the strengths of the Ising interaction and the transverse fields, respectively; and h_i is a set of local z-fields that break integrability of the model. Compared to a digitized implementation of the transverse Ising Hamiltonian (see fig. S11 for experimental data of this approach), the periodic (i.e., Floquet) evolution here generates faster dynamics in real time and is advantageous given the finite coherence times of the gubits. Under such a drive, the Hilbert space of the system may be described by the eigenstates of \hat{U}_F whose eigenvalues lie on a unit circle, as illustrated in the right panel of Fig. 1B.

Given that there is no ground state in a Floquet system, the twofold degeneracy of the ground state in the Kitaev model instead becomes a pairing of eigenstates across the entire spectrum. In our work, we fix J=1/2, wherein the Floquet system, in the integrable limit $h_j=0$, has \mathbb{Z}_2 spin-flip symmetry and exhibits two phases with distinct spectral pairings. For the phase characterized by g>0.5, which is the focus of the main text, the quasienergy levels



shown on a unit circle according to their quasienergies. **(C)** $\langle \hat{Z}_j(t) \rangle$ as a function of t and qubit location Q_j . The initial state is a random product state, $|0101001...\rangle$. (Inset) $\langle \hat{Z}_j(t) \rangle$ for the three leftmost and rightmost qubits, between t=50 and t=200. **(D)** $\langle \hat{Z}_j(t) \rangle$ for the two edge qubits j=1 and 47 (left panel) and two qubits within the bulk j=16 and 32 (right panel). Top axis for each plot indicates real time, calculated on the basis of the time needed to execute \hat{U}_F (93 ns). Locations for the qubits shown in this panel are also indicated by colored arrows in (C).

have a π -pairing (Fig. 1B, right panel): Every many-body eigenstate of the $\hat{U}_{\rm F}$ with quasi-energy θ has a "partner" state with quasi-energy $\theta + \pi$ (34). The transition between any paired eigenstates is enabled by an application of the so-called π -MEMs, $\hat{\chi}_{\rm L}$ and $\hat{\chi}_{\rm R}$ (35, 36). The π -MEMs anticommute with $\hat{U}_{\rm F}$ in the large L limit

$$\hat{\chi}_{\mathrm{L}}\hat{U}_{\mathrm{F}} = -\hat{U}_{\mathrm{F}}\hat{\chi}_{\mathrm{L}}, \hat{\chi}_{\mathrm{R}}\hat{U}_{\mathrm{F}} = -\hat{U}_{\mathrm{F}}\hat{\chi}_{\mathrm{R}} \qquad (2)$$

At g < 0.5, the eigenspectrum of \hat{U}_F has a double degeneracy, that is, each eigenstate has a partner state with the same quasienergy. Here, the transition between paired eigenstates is described by two so-called 0-MEMs that commute with \hat{U}_F . Experimental data for this regime, which is analogous to the ferromagnetic phase of the transverse Ising model, are shown in fig. S10. At the critical point g = 0.5, the eigenstates are distributed

uniformly on the unit circle with a gap of π/L , which vanishes in the limit $L = \infty$.

In the presence of finite local fields $h_j \neq 0$, \hat{U}_F is no longer integrable and the \mathbb{Z}_2 symmetry is also broken. We begin by searching for signatures of stable edge modes in this regime, focusing on the \hat{Z} operators that, in the JWT, have large overlap with MEMs on the edge (Fig. 1A). Figure 1C shows experimental measurements of $\langle \hat{Z}_j(t) \rangle$ for all qubits

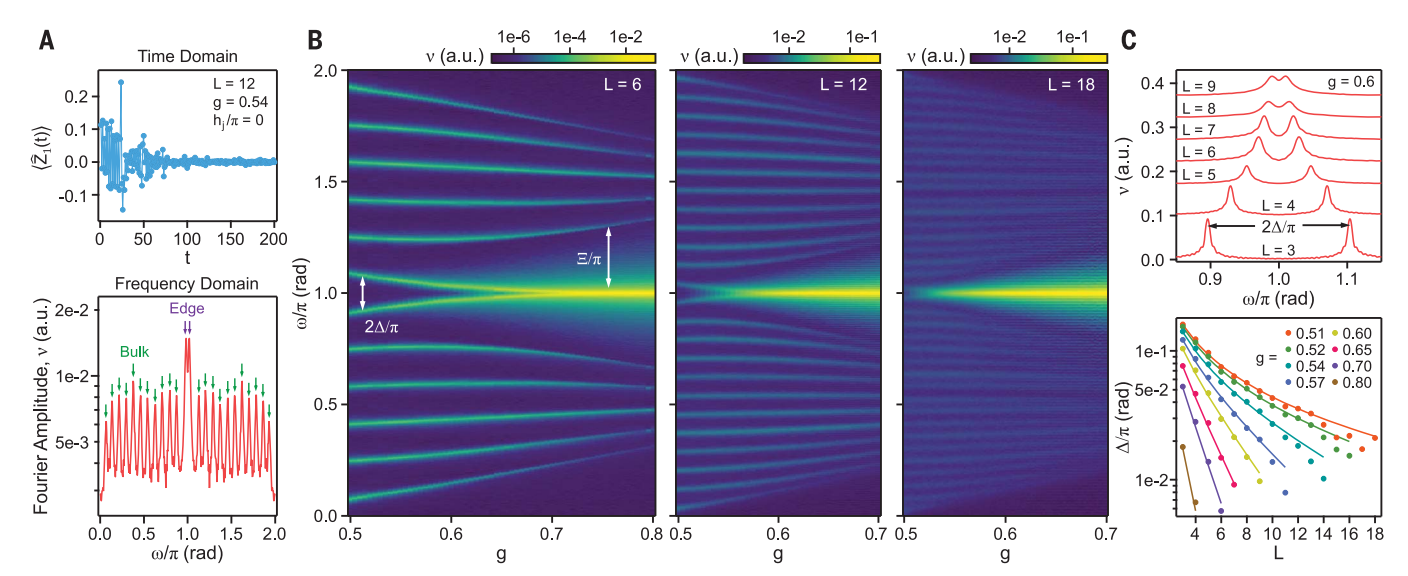


Fig. 2. Quasienergy spectroscopy. (**A**) (Top) $\langle \hat{Z}_1(t) \rangle$ measured in the integrable limit $h_j = 0$ and system size L = 12. (Bottom) Frequency-dependent amplitude $\mathbf{v}(\mathbf{\omega})$ of the Fourier transform of $\langle \hat{Z}_1(t) \rangle$ in the top panel. The arrows indicate the single-particle quasienergy peaks for the bulk and edge fermionic modes. a.u., arbitrary units. (**B**) \mathbf{v} as a function of both frequency $\mathbf{\omega}/\pi$ and g, measured for three different values of L. In all cases, $h_i = 0$. To obtain the

spectra, $\langle \hat{Z}_1(t) \rangle$ is measured up to t=300, 200, and 150 cycles for L=6, 12, and 18, respectively. **(C)** (Top) $\nu(\omega)$ for different L, showing the quasienergy peaks of the hybridized MEMs with a splitting $2\Delta/\pi$. Data are offset for clarity. (Bottom) Δ/π measured as a function of L at different values of g. Solid lines represent exact numerical results from diagonalizing \hat{U}_F in the fermionic basis (33). Random product states are used as initial states in all measurements.

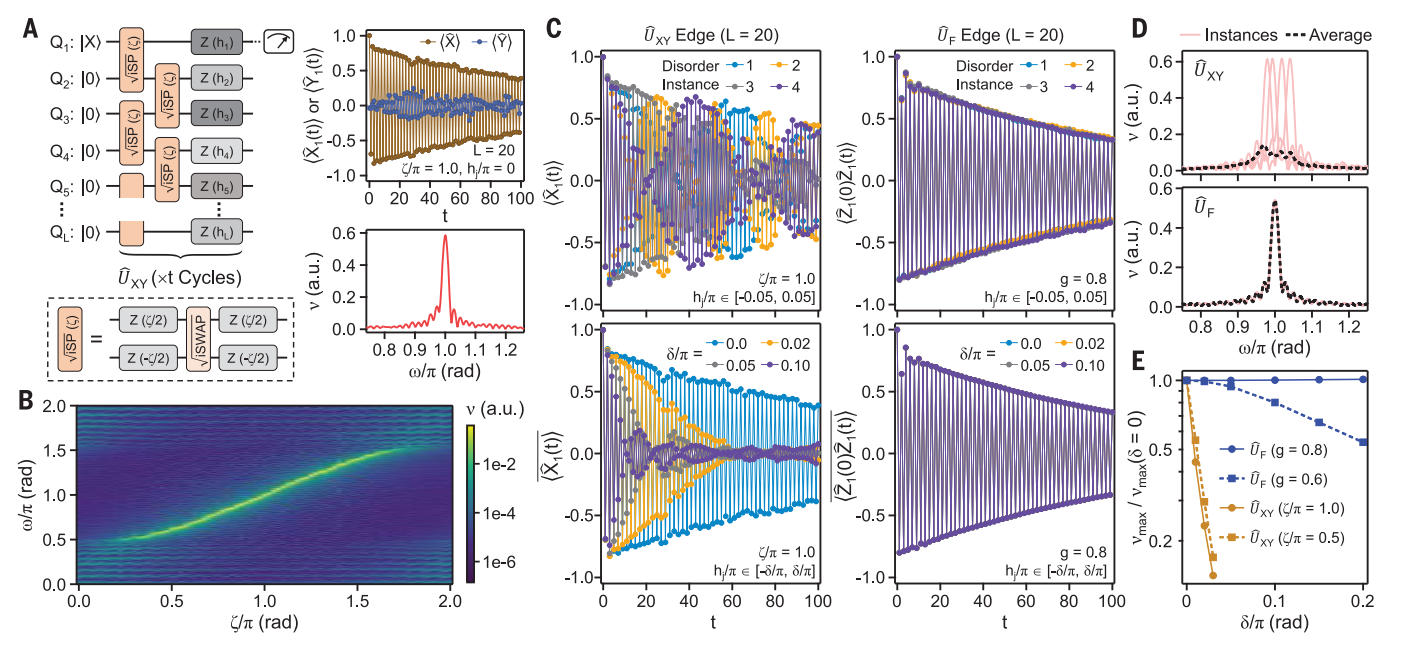


Fig. 3. Low-frequency noise resilience of MEMs and comparison with unprotected edge modes. (A) (Left) Quantum circuit corresponding to the XY model, where an identical cycle unitary $\hat{U}_{\rm XY}$ is applied t times. (Right) Top panel shows $\langle \hat{X}_1(t) \rangle$ and $\langle \hat{Y}_1(t) \rangle$ measured at Q_1 , with the control parameter $\zeta/\pi=1.0$ and no disorder $h_j/\pi=0$. Bottom panel shows the Fourier spectrum $\mathbf{v}(\omega)$ of $\langle \hat{X}_1(t) \rangle + i \langle \hat{Y}_1(t) \rangle$. (B) $\mathbf{v}(\omega)$ as a function of ω/π and ζ for the $\hat{U}_{\rm XY}$ model, where $\langle \hat{X}_1(t) \rangle$ and $\langle \hat{Y}_1(t) \rangle$ are measured up to t=100. (C) (Top panels) $\langle \hat{X}_1(t) \rangle$ ($\langle \hat{Z}_1(0)\hat{Z}_1(t) \rangle$) for the $\hat{U}_{\rm XY}$ ($\hat{U}_{\rm F}$) edge modes, measured for four different disorder

realizations with $h_{j'}/\pi \in [-0.05,0.05]$. (Bottom panels) Disorder-averaged $\langle \hat{X}_1(t) \rangle$ ($\langle \hat{Z}_1(0) \hat{Z}_1(t) \rangle$) for the $\hat{U}_{XY}(\hat{U}_F)$ edge mode, shown over four different disorder strengths δ . Eighty disorder instances $h_{j'}/\pi \in [-\delta/\pi, \delta/\pi]$ are used for averaging in each case, and the initial states are additionally randomized between instances for \hat{U}_F . (**D**) Red lines: Fourier spectra $v(\omega)$ obtained from the disorder instances in the upper panels of (C). Black lines: $v(\omega)$ for the disorder-averaged observables ($\delta = 0.05$) in the lower panels of (C). (**E**) Maximum Fourier amplitude v_{max} as a function of δ . Data are normalized by v_{max} at $\delta = 0$.

in the chain, where we have chosen h_j/π from a random uniform distribution [-1,1] to maximize the effect of integrability breaking. We observe a stark contrast in the behavior of the edge qubits, Q_1 and Q_{47} , and qubits within the

chain, Q_2 to Q_{46} . Whereas $\langle Z_j(t) \rangle$ decays rapidly to 0 after ~20 cycles (~2 μ s) for any qubit in the bulk, $\langle \hat{Z}_j(t) \rangle$ decays much more slowly for the edge qubits. In addition, $\langle \hat{Z}_j(t) \rangle$ for each edge qubit shows a subharmonic oscillation

at a period twice that of the drive \hat{U}_F , because each application of \hat{U}_F changes the sign of $\hat{\chi}_{L,R}$ owing to their anticommutation (Eq. 2).

The bulk-edge difference is further illustrated in Fig. 1D, where data for four qubits

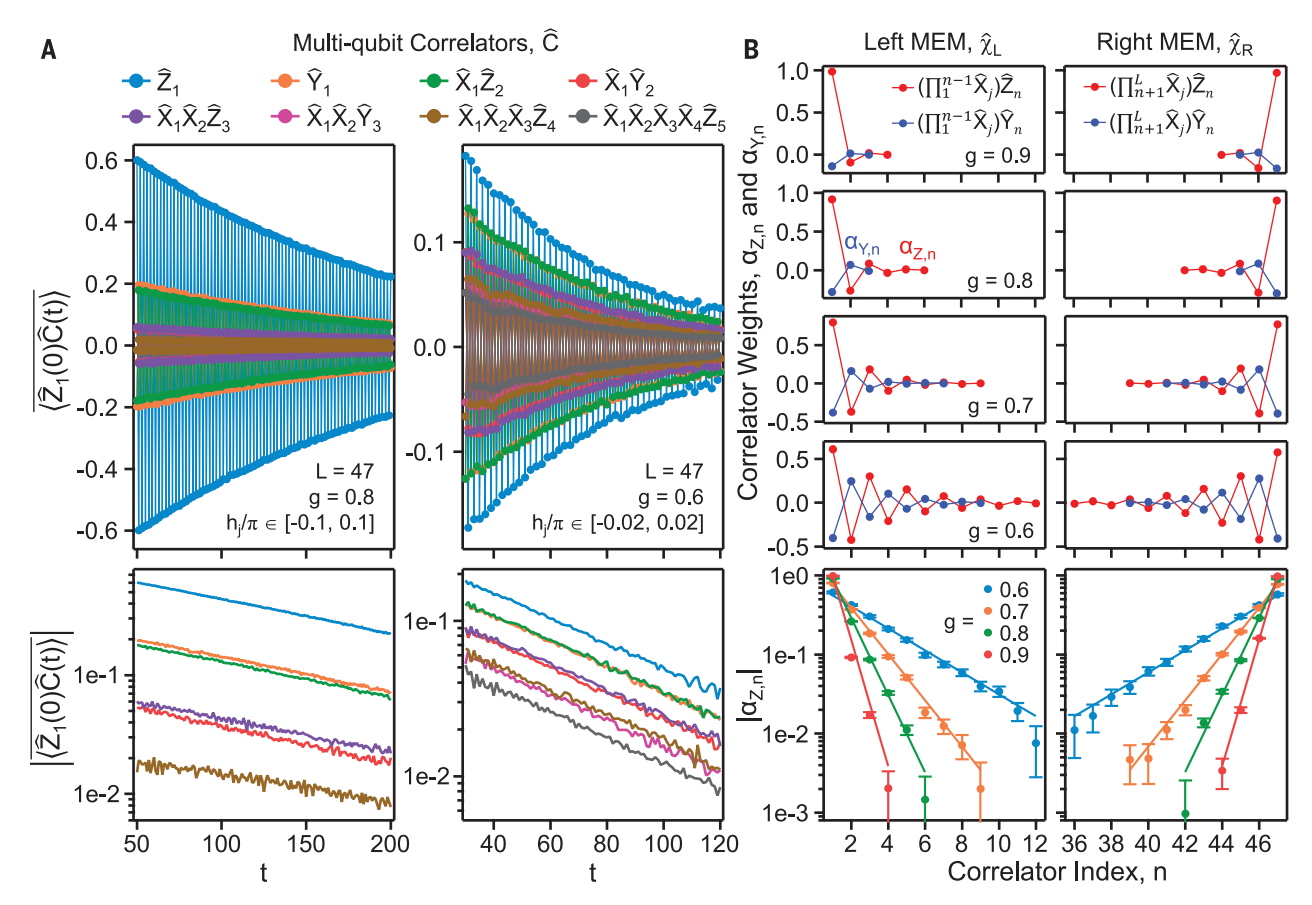


Fig. 4. Reconstructing the Pauli operator expansion of MEMs. (**A**) (Top panels) Correlators $\langle \hat{Z}_1(0)\hat{C}(t)\rangle$ for g=0.8 and g=0.6, with the compositions of $\hat{C}(t)$ shown in the legend. Here, the g=0.8 (g=0.6) data are averaged over 10 (12) disorder realizations and initial random product states. Bottom panels show the absolute values of the correlators, $|\hat{Z}_1(0)\hat{C}(t)|$. (**B**) The top eight panels show

experimentally reconstructed Pauli operator expansion of the MEMs $\hat{\chi}_{L,R}$; $\alpha_{Z,n}$ and $\alpha_{Y,n}$ correspond to the coefficients of the Pauli operators shown in the legends. The bottom two panels show experimental values of $|\alpha_{Z,n}|$ (points) and theoretical predictions (solid lines). Error bars correspond to statistical uncertainty stemming from single-shot measurements [see methods (33)].

are shown. The lifetimes of the edge modes, which include contributions from both external decoherence effects and internal nonintegrable dynamics, are extracted by fitting the envelope of $\langle \hat{Z}_1(t) \rangle (\langle \hat{Z}_{47}(t) \rangle)$ to an exponential (fig. S8) and found to be 19.5 μ s (17.2 μ s) for Q_1 (Q_{47}). These values are close to the typical single-qubit relaxation time T_1 = 22.2 μ s on the device—a preliminary indication that the MEMs are resilient toward integrability and symmetry-breaking fields as well as dephasing effects such as low-frequency noise.

Recent theoretical works have suggested that the resilience of the edge modes toward nonintegrable dynamics is a result of prethermalization (37–41). Unlike thermalizing systems, which monotonically decay to ergodic states over time, a prethermal system relaxes first to a metastable state before decaying to ergodic states. A common mechanism for prethermalization is the existence of spectral gaps, which make relaxation processes driven by integrability-breaking perturbations off-resonant, thereby preventing energy absorption. To experimentally establish prethermalization

in our system, we characterize the excitation spectrum in the integrable limit, $h_i = 0$. Here, the many-body spectrum of \hat{U}_{F} may be constructed from a total of 2L energy quanta, corresponding to the quasienergies of noninteracting Bogoliubov fermionic quasiparticles in the fermionic representation of \hat{U}_F . These quasienergies can be obtained through a Fourier analysis of timedomain signals (42, 43) [see supplementary text sections III and V (33)]. Figure 2A shows measurements of $\langle \hat{Z}_1(t) \rangle (h_i = 0)$ for a short chain L = 12. The time evolution for $\langle \hat{Z}_1(t) \rangle$ is now seemingly featureless, which results from interference between different eigenmodes of \hat{U}_F . To obtain the quasienergies, a Fourier transform of the time-domain data is then performed (Fig. 2A. bottom). The Fourier spectrum $v(\omega)$ reveals a total of 2L distinct peaks at values of ω corresponding to the quasienergies of the 2Lnoninteracting fermionic modes in the system.

The two dominant peaks close to $\omega = \pi$ in the spectrum of Fig. 2A are associated with the MEMs, which are split in quasienergy because of their hybridization in this short chain. To confirm this interpretation, we change the

localization length ξ of the MEMs by tuning gand measure the spectra over three different system sizes. The results, shown in Fig. 2B, reveal two important features: First, we observe that the quasienergy splitting 2Δ of the two MEMs decreases as g increases. This is caused by a reduced ξ that leads to weaker hybridization between $\hat{\chi}_L$ and $\hat{\chi}_R$. Second, we observe a finite quasienergy gap Ξ between the MEMs and the other bulk fermionic modes, which increases at larger g. This quasienergy gap, which crucially remains open as L increases, suppresses transitions between bulk and edge states and is the key to protecting the MEMs against integrability-breaking fields. Further discussion of this prethermalization mechanism is presented in supplementary text section IV (33).

Although the bulk gap protects the MEMs from internal thermalization, the finite quasienergy difference 2Δ between the two MEMs is sensitive to disorder fluctuations. Such a sensitivity may lead to dephasing of the MEMs through low-frequency noise (20), as shown by fig. S5. This effect may be suppressed by

reducing the hybridization between $\hat{\chi}_L$ and $\hat{\chi}_R$, which is achievable through increasing either g (Fig. 2B) or L. The dependence of Δ on L is mapped out in detail by the experimental measurements shown in Fig. 2C. We observe that for g>0.6, Δ is exponentially suppressed by larger L, in agreement with theory (33). For g<0.6, the suppression is no longer exponential, given the proximity to the phase transition point g=0.5, where the bulk gap closes. We also find excellent agreement between exact numerical results and experimental measurements even for $\Delta/\pi\approx0.01$, which is a result of accurate gate calibrations described in (33).

We next perform a systematic study on the low-frequency noise resilience of the MEMs for a moderately long chain, L = 20. To examine the role of symmetry in noise protection, we have also experimentally realized edge modes in a different periodic circuit with a cycle unitary \hat{U}_{XY} that does not have \mathbb{Z}_2 symmetry. As illustrated in Fig. 3A, \hat{U}_{XY} consists of two layers of two-qubit gates applied between all nearest-neighbor qubits, $\sqrt{iSP(\zeta)} = e^{-i\frac{\zeta}{4}(\hat{Z}_j - \hat{Z}_{j+1})} e^{-i\frac{\pi}{4}(\hat{\sigma}_j^+ \hat{\sigma}_{j+1}^- + \hat{\sigma}_j^- \hat{\sigma}_{j+1}^+)} e^{-i\frac{\zeta}{4}(\hat{Z}_j - \hat{Z}_{j+1})}$, where $\hat{\sigma}^{+,-}$ denotes Pauli raising and lowering operators. In the single-excitation subspace, U_{XY} has L eigenmodes, including two localized edge modes [see appendix E of (44)] for control parameter $\zeta/\pi \in [0.25, 1.75]$. The leading order terms in the Pauli operator expansion of the edge modes are $\hat{\sigma}_{L}^{+}$ and $\hat{\sigma}_{L}^{+}$, respectively.

To probe one of the edge modes for \hat{U}_{XY} , we prepare the system in a superposition state $\frac{1}{\sqrt{2}}(|0000...\rangle + |1000...\rangle)$ to maximize the initial value $\langle \hat{\sigma}_1^+(t=0) \rangle = 1$. We then apply \hat{U}_{XY} t times before measuring the time-dependent observable $\langle \hat{\sigma}_1^+(t) \rangle = \langle \hat{X}_1(t) \rangle + i \langle \hat{Y}_1(t) \rangle$, which precesses at a frequency corresponding to the quasienergy of the edge mode. Example experiment data and the corresponding Fourier spectrum $v(\omega)$ for $\zeta/\pi = 1.0$ are both shown in Fig. 3A, demonstrating a slowly decaying subharmonic response and a quasienergy peak at $\omega = \pi$ that are similar to those of the MEMs of the $U_{\rm F}$ model. Figure 3B shows experimentally measured v as a function of both ζ and ω . At $0.25 \lesssim \zeta/\pi \lesssim 1.75$, we observe a dominant quasienergy peak that corresponds to an edge mode and is separated from the L-2 bulk modes, visible as smaller peaks outside the range 0.5 < ω_{π} < 1.5, by spectral gaps akin to the bulk gap Ξ of the $\hat{U}_{\rm F}$ model. Despite these apparent similarities, a crucial distinction exists between the two models: The quasienergy of the \hat{U}_{XY} edge mode is first-order sensitive to ζ at all values of ζ , whereas the quasienergy of the $\hat{U}_{\rm F}$ edge mode asymptotically approaches π as g increases. This distinction stems from the lack of \mathbb{Z}_2 symmetry in \hat{U}_{XY} and leads to drastically different robustness of the two models toward low-frequency noise in h_i , which we explore next.

The upper panels of Fig. 3C show $\langle \hat{X}_1(t) \rangle$ $(\langle \hat{Z}_1(0)\hat{Z}_1(t) \rangle)$ of the $\hat{U}_{XY}(\hat{U}_F)$ model, mea-

sured for four different realizations of h_i/π that are uniformly chosen from $[-\delta, \delta]$. Here, the autocorrelator $\langle \hat{Z}_1(0)\hat{Z}_1(t)\rangle$ differs from $\langle \hat{Z}_1(t) \rangle$ only by a random \pm sign given by the initial state of Q_1 , and $\delta = 0.05$ is a disorder strength chosen to be comparable to the lowfrequency fluctuation of the quantum device. We observe that $\langle \hat{X}_1(t) \rangle$ exhibits beating patterns that depend sensitively on the disorder realization. This is a result of the first-order sensitivity toward control parameters demonstrated in Fig. 3B. On the other hand, $\langle \hat{Z}_1(0)\hat{Z}_1(t)\rangle$ is virtually unchanged between different disorder realizations. The impact of low-frequency noise on each edge mode realization is then emulated by averaging the corresponding observable over an ensemble of disorder realizations, which mimics the process of dephasing. The disorderaveraged $\langle \hat{X}_1(t) \rangle$ in the \hat{U}_{XY} model, shown in the lower panel of Fig. 3C, decays significantly faster as the disorder strength δ increases. On the other hand, $\langle \hat{Z}_1(0)\hat{Z}_1(t)\rangle$ in the $\hat{U}_{\rm F}$ model remains unchanged over δ .

The sensitivity of the two edge mode realizations toward low-frequency noise is further elucidated by inspecting the Fourier spectrum $v(\omega)$ of each disorder realization, shown in Fig. 3D. Here, we observe that the quasienergy peak for the \hat{U}_{XY} edge mode is different for each disorder realization, resulting in a broadened spectrum with a lower peak height upon averaging. On the other hand, the quasienergy peak for $\hat{U}_{\rm F}$ remains stable at $\omega = \pi$, irrespective of disorder realizations. Lastly, we measure the disorder-averaged quasienergy peak height, $v_{\text{max}} = \text{Max}[v(\omega)]$, and show the results in Fig. 3E. For the \hat{U}_{XY} model, we observe that v_{max} decays exponentially as a function of δ irrespective of ζ . For the $\hat{U}_{\rm F}$ model, $v_{\rm max}$ is completely insensitive to δ for sufficiently localized MEMs (g = 0.8) and remains insensitive for small δ < 0.05 even in the more delocalized regime g = 0.6. These results highlight the critical role of symmetry in stabilizing the quasienergies of MEMs and protecting their lifetimes against low-frequency noise.

Finally, using the full L=47 qubit chain, we demonstrate an error-mitigation strategy for accurately reconstructing the Pauli operator expansion of $\hat{\chi}_{L,R}$ in the presence of noise. Figure 4A shows the late-time evolution of eight multiqubit Pauli operators \hat{C} entering the JWT of $\hat{\chi}_{L,R}$, experimentally obtained by rotating each qubit linto the appropriate basis followed by multi-

qubit readout. We observe that each $\hat{Z}_1(0)\hat{C}(t)$

exhibits a similar subharmonic response, with an amplitude that decreases when \hat{C} incorporates more qubits and has less overlap with $\hat{\chi}_{\rm L,R}$ (Fig. 1A). Operators ending with \hat{Y} also show smaller amplitudes than those ending with \hat{Z} because they have no overlap with $\hat{\chi}_{\rm L,R}$ in the time-independent transverse Ising model and only arise as corrections to the JWT of

 $\hat{\chi}_{\text{L,R}}$ as a consequence of the time-dependent, periodic dynamics. Notably, as shown also in Fig. 4A, the absolute values (i.e., magnitudes) of these operators, $|\hat{Z}_1(0)\hat{C}(t)|$, exhibit nearly identical decay rates despite their different lengths and compositions.

The observation in Fig. 4A is contrary to naïve expectations, wherein the decay rate of a quantum operator is expected to scale with the number of qubits it incorporates. The result may be qualitatively understood by the fact that $\hat{\chi}_L$ and $\hat{\chi}_R$ anticommute with \hat{U}_F (Eq. 2) and are conserved under the periodic dynamics. Even though external decoherence and integrability-breaking fields violate this commutation, $\hat{\chi}_{L,R}$ remains a slowly decaying mode [see supplementary text section VII (33)]. As a result, any multiqubit operator having a finite overlap with $\hat{\chi}_{L,R}$ will exhibit a slow-decaying expectation value in its late-time dynamics, with an amplitude proportional to the overlap.

The uniform decay rates of $\hat{Z}_1(0)\hat{C}(t)$ inform an experimental strategy for reconstructing the expansion of the MEMs in the Pauli operator basis

$$\hat{\chi}_{\mathrm{L,R}} = \sum_{n=1}^{L} \left[\alpha_{\mathrm{Z},n} \left(\prod_{j=M}^{N} \hat{X}_{j} \right) \hat{Z}_{n} + \alpha_{\mathrm{Y},n} \left(\prod_{j=M}^{N} \hat{X}_{j} \right) \hat{Y}_{n} \right]$$

$$(3)$$

where the products over j have limits N=n-1 and M=1 for $\hat{\chi}_L$, and N=L and M=n+1 for $\hat{\chi}_R$ (45). The coefficients $\alpha_{Z,n}$ and $\alpha_{Y,n}$ normalize to unity for $L=\infty$: $\sum_n \left|\alpha_{Z,n}\right|^2 + \left|\alpha_{Y,n}\right|^2 = 1$. To estimate their values, we measure different $\hat{Z}_1(0)\hat{C}(t)$ at 10 late-time cycles. The average value of each operator and the normalization condition allow us to determine the ideal values of $\alpha_{Z,n}$ and $\alpha_{Y,n}$ [see methods and supplementary text section VI (33) for details].

The experimentally measured coefficients, shown in Fig. 4B for four values of g, both oscillate in sign and decay exponentially as n moves away from the edge. The decay rate is also observed to decrease as g approaches the critical value g=0.5. This is a result of the fact that the decay constant for the coefficients is the localization length ξ of the MEMs, which diverges at g=0.5 [see supplementary text section III (33)]. A comparison between theoretical and experimental values of $|\alpha_{Z,n}|$ is shown in the bottom panels of Fig. 4B, where good agreement is found over a span of nearly three orders of magnitude.

In this study, we simulate MEMs using a system of driven transmon qubits and comprehensively study their symmetry protection against noise in their solid-state environment. We find that the degree of protection sensitively depends on the physical characteristic of the noise and generally does not extend to noise that breaks the underlying symmetry, such as T_1 decay of the transmon qubits. We also find that, because of a prethermalization

mechanism, the MEMs in our system are protected against certain noise that seemingly violates \mathbb{Z}_2 symmetry, for example, local \hat{Z} fluctuations. These results highlight the complex interplay between physical noise and protection and indicate the crucial importance of testing symmetry against open-system dynamics in any experimental platform. Furthermore, we find that even in the presence of decoherence, the Pauli expansion of conserved quantities such as MEMs can be accurately determined by measuring and renormalizing late-time expectation values of Pauli operators. This error-mitigation strategy may be applied to study integrals of motion in physical models that are more difficult to compute classically. Preliminary results on nonintegrable dynamics are shown in fig. S7.

REFERENCES AND NOTES

- 1. P. Zanardi, M. Rasetti, Phys. Rev. Lett. 79, 3306-3309 (1997).
- D. A. Lidar, I. L. Chuang, K. B. Whaley, *Phys. Rev. Lett.* 81, 2594–2597 (1998).
- D. Bacon, J. Kempe, D. A. Lidar, K. B. Whaley, *Phys. Rev. Lett.* 85, 1758–1761 (2000).
- 4. A. Y. Kitaev, Ann. Phys. 303, 2-30 (2003).
- C. Nayak, S. H. Simon, A. Stern, M. Freedman, S. Das Sarma, Rev. Mod. Phys. 80, 1083–1159 (2008).
- A. G. Fowler, M. Mariantoni, J. M. Martinis, A. N. Cleland, Phys. Rev. A 86, 032324 (2012).
- A. Y. Kitaev, Phys. Uspekhi 44, 131–136 (2001).
- N. Read, D. Green, Phys. Rev. B Condens. Matter 61, 10267–10297 (2000).
- R. M. Lutchyn, J. D. Sau, S. Das Sarma, Phys. Rev. Lett. 105, 077001 (2010).
- 10. Y.Oreg, G. Refael, F. von Oppen, Phys. Rev. Lett. 105, 177002 (2010).
- 11. V. Mourik et al., Science **336**, 1003–1007 (2012).
- 12. L. P. Rokhinson, X. Liu, J. K. Furdyna, Nat. Phys. 8, 795-799 (2012).
- 13. A. Das et al., Nat. Phys. 8, 887-895 (2012).

- 14. S. Nadj-Perge et al., Science 346, 602-607 (2014).
- 15. S. M. Albrecht et al., Nature 531, 206-209 (2016).
- 16. P. Yu et al., Nat. Phys. 17, 482-488 (2021).
- G. Goldstein, C. Chamon, Phys. Rev. B Condens. Matter Mater. Phys. 84, 205109 (2011).
- M. Cheng, R. M. Lutchyn, S. Das Sarma, Phys. Rev. B Condens. Matter Mater. Phys. 85, 165124 (2012).
- J. C. Budich, S. Walter, B. Trauzettel, Phys. Rev. B Condens. Matter Mater. Phys. 85, 121405 (2012).
- C. Knapp, T. Karzig, R. M. Lutchyn, C. Nayak, *Phys. Rev. B* 97, 125404 (2018).
- E. M. Levenson-Falk, F. Kos, R. Vijay, L. Glazman, I. Siddiqi, *Phys. Rev. Lett.* 112, 047002 (2014).
- 22. B. Feldman et al., Nat. Phys. 13, 286-291 (2016)
- 23. K. Serniak et al., Phys. Rev. Lett. 121, 157701 (2018).
- 24. M. Hays et al., Phys. Rev. Lett. 121, 047001 (2018).
- 25. R. Blatt, C. F. Roos, *Nat. Phys.* **8**, 277–284 (2012). 26. C. Gross, I. Bloch, *Science* **357**, 995–1001 (2017).
- 27. I. Carusotto *et al.*, *Nat. Phys.* **16**, 268–279 (2020).
- 28. E. Lieb, T. Schultz, D. Mattis, Ann. Phys. 16, 407-466 (1961).
- 29. L. S. Levitov, T. P. Orlando, J. B. Majer, J. E. Mooij, arXiv:cond-mat/0108266 [cond-mat.mes-hall] (2001).
- 30. J. Q. You, Z. D. Wang, W. Zhang, F. Nori, Sci. Rep. 4, 5535 (2014).
- 31. J.-S. Xu et al., Sci. Adv. 4, eaat6533 (2018).
- 32. M. I. Dykman, Phys. Rev. A 100, 042101 (2019).
- 33. Materials and methods are available as supplementary materials.
- V. Khemani, A. Lazarides, R. Moessner, S. L. Sondhi, *Phys. Rev. Lett.* 116, 250401 (2016).
- 35. M. Thakurathi, A. A. Patel, D. Sen, A. Dutta, *Phys. Rev. B Condens. Matter Mater. Phys.* **88**, 155133 (2013).
- D. J. Yates, F. H. L. Essler, A. Mitra, Phys. Rev. B 99, 205419 (2019).
- 37. P. Fendley, J. Phys. A Math. Theor. 49, 30LT01 (2016).
- 38. D. Abanin, W. De Roeck, W. W. Ho, F. Huveneers, Commun. Math. Phys. **354**, 809–827 (2017).
- 39. T. Mori, T. Kuwahara, K. Saito, Phys. Rev. Lett. 116, 120401 (2016).
- 40. D. V. Else, B. Bauer, C. Nayak, Phys. Rev. X 7, 011026 (2017).
- D. V. Else, P. Fendley, J. Kemp, C. Nayak, *Phys. Rev. X* 7, 041062 (2017).
- 42. P. Roushan et al., Science 358, 1175-1179 (2017).
- 43. N. Harle, O. Shtanko, R. Movassagh, arXiv:2203.15083 [quant-ph] (2022).
- 44. C. Neill et al., Nature 594, 508-512 (2021).

- 45. In Eq. 3, product terms $\prod_{i=M}^N \hat{Y}_i$ with N < M should be treated as identity \hat{I} . Additionally, the JWT of $\hat{\chi}_R$ should, in principle, have higher weights in longer Pauli strings, with the dominant string being $\left(\prod_{i=1}^{l-1}\hat{X}_i\right)\hat{Y}_L$. This is equivalent to \hat{Z}_L up to the parity transformation $\prod_{i=1}^{l}\hat{X}_i$, which commutes with \hat{U}_F . In Eq. 3, $\hat{\chi}_R$ is expressed in this alternative form and has a leading term $\alpha_Z L \hat{Z}_L$. Such a basis requires measurements of shorter Pauli strines.
- Google Quantum AI, Data and Simulation Code for "Noise Resilient Edge Modes on a Chain of Superconducting Qubits," version 1, Zenodo (2022); https://doi.org/10.5281/zenodo.7190882.

ACKNOWLEDGMENTS

We have benefited from discussions with M. H. Devoret, L. G. Dias, I. K. Drozdov, P. Ghaemi, and A. Rahmani, Funding: D.B. is a CIFAR Associate Fellow in the Quantum Information Science Program. Author contributions: D.A.A. and V.Sm. conceived of the project. X.M., D.A.A., and V.Sm. designed the experiment. X.M. executed the experiment. P.R., X.M., D.A.A., M.So., and M.Y.N. performed analysis of the experimental results, K.W.L. and B.F. contributed to measurements in the supplementary materials. X.M., P.R., and D.A.A. wrote the manuscript. V.Sm. and P.R. led and coordinated the project. Infrastructure support was provided by Google Quantum Al. All authors contributed to revising the manuscript and the supplementary materials. Competing interests: The authors declare no competing interests. Data and materials availability: Experimental data shown in the main text and supplementary materials, as well as simulation software code, are available in Zenodo (46). License information: Copyright @ 2022 the authors, some rights reserved; exclusive licensee American Association for the Advancement of Science. No claim to original US government works. https://www.science.org/about/science-licenses-journal-article-reuse

SUPPLEMENTARY MATERIALS

science.org/doi/10.1126/science.abq5769 Materials and Methods Supplementary Text Figs. S1 to S15 References (47–60)

Submitted 17 April 2022; accepted 21 October 2022 10.1126/science.abq5769

Mi et al., Science **378**, 785-790 (2022) 18 November 2022 **6 of 6**



Noise-resilient edge modes on a chain of superconducting qubits

X. Mi, M. Sonner, M. Y. Niu, K. W. Lee, B. Foxen, R. Acharya, I. Aleiner, T. I. Andersen, F. Arute, K. Arya, A. Asfaw, J. Atalaya, J. C. Bardin, J. Basso, A. Bengtsson, G. Bortoli, A. Bourassa, L. Brill, M. Broughton, B. B. Buckley, D. A. Buell, B. Burkett, N. Bushnell, Z. Chen, B. Chiaro, R. Collins, P. Conner, W. Courtney, A. L. Crook, D. M. Debroy, S. Demura, A. Dunsworth, D. Eppens, C. Erickson, L. Faoro, E. Farhi, R. Fatemi, L. Flores, E. Forati, A. G. Fowler, W. Giang, C. Gidney, D. Gilboa, M. Giustina, A. G. Dau, J. A. Gross, S. Habegger, M. P. Harrigan, M. Hoffmann, S. Hong, T. Huang, A. Huff, W. J. Huggins, L. B. Ioffe, S. V. Isakov, J. Iveland, E. Jeffrey, Z. Jiang, C. Jones, D. Kafri, K. Kechedzhi, T. Khattar, S. Kim, A. Y. Kitaev, P. V. Klimov, A. R. Klots, A. N. Korotkov, F. Kostritsa, J. M. Kreikebaum, D. Landhuis, P. Laptev, K.-M. Lau, J. Lee, L. Laws, W. Liu, A. Locharla, O. Martin, J. R. McClean, M. McEwen, B. Meurer Costa, K. C. Miao, M. Mohseni, S. Montazeri, A. Morvan, E. Mount, W. Mruczkiewicz, O. Naaman, M. Neeley, C. Neill, M. Newman, T. E. O'Brien, A. Opremcak, A. Petukhov, R. Potter, C. Quintana, N. C. Rubin, N. Saei, D. Sank, K. Sankaragomathi, K. J. Satzinger, C. Schuster, M. J. Shearn, V. Shvarts, D. Strain, Y. Su, M. Szalay, G. Vidal, B. Villalonga, C. Vollgraff-Heidweiller, T. White, Z. Yao, P. Yeh, J. Yoo, A. Zalcman, Y. Zhang, N. Zhu, H. Neven, D. Bacon, J. Hilton, E. Lucero, R. Babbush, S. Boixo, A. Megrant, Y. Chen, J. Kelly, V. Smelyanskiy, D. A. Abanin, and P. Roushan

Science 378 (6621), . DOI: 10.1126/science.abq5769

Tough edges

The dynamics of quantum many-body systems can be profoundly affected by their interaction with the environment. This includes systems that have topological protection from certain kinds of perturbations due to symmetry. Mi *et al.* studied the interplay between symmetry and noise using a chain of 47 superconducting qubits. They implemented a periodically driven transverse Ising spin model, and found that the system's edge modes were surprisingly resilient to some types of symmetry-breaking noise. —JS

View the article online

https://www.science.org/doi/10.1126/science.abq5769

Permissions

https://www.science.org/help/reprints-and-permissions

Use of this article is subject to the Terms of service